

# Theoretical analysis of damping effects of guided elastic waves at solid/fluid interfaces

S. Ballandras,<sup>a)</sup> A. Reinhardt, A. Khelif, M. Wilm, V. Laude, W. Daniau, and V. Blondeau-Patissier

*Institut FEMTO-ST, UMR CNRS-UFC-ENSMM-UTBM 6174, Département LPMO, 32 Avenue de l'Observatoire, F-25044 Besançon Cedex, France*

(Received 7 June 2005; accepted 14 December 2005; published online 14 March 2006)

A theoretical description of ideal and viscous fluid media is proposed to address the problem of modeling damping effects of surface acoustic waves and more generally of any guided elastic waves at the interface between viscous fluids and solids. It is based on the Fahmy-Adler eigenvalue representation of the elastic propagation problem, adapted to provide Green's function of the considered media. It takes advantage of previous efforts developed to numerically stabilize Green's-function computation process. This function is used to compute a harmonic admittance according to the Blötekaer approach. The influence of acoustic radiation and viscosity effects on different kinds of waves excited on various substrates is reported and discussed. © 2006 American Institute of Physics. [DOI: 10.1063/1.2168242]

## I. INTRODUCTION

Surface acoustic waves (SAWs) can be excited at the surface of any solid material. These waves may exhibit elliptic as well as pure shear polarizations (case of isotropic media), but the practical case of wave propagation at the surface of anisotropic material generally yields combinations of pure polarization, except along the given crystal or symmetry axes.<sup>1</sup> True SAWs are assumed to propagate without any losses along the guiding surface, providing a nice opportunity to manufacture low loss devices such as filters and resonators. However, it is also known that best quality factors and/or smallest insertion losses of SAW devices are obtained using packages closed under vacuum to avoid leakage due to acoustic radiation in air. The use of SAW devices for the development of sensors immersed in fluid media has also been widely investigated. For instance, Rayleigh waves are known to be dramatically damped by water but pure shear waves are often considered capable to exist even when their propagation substrate is loaded by a liquid. Theoretical analysis of SAW excitation and propagation under such operating conditions requires the adaptation of existing simulation tools to provide a reliable description of the induced effects by the nature of the surrounding medium on the SAW device response.

In the proposed analysis, the way Green's function and the harmonic admittance can be used in that matter is described. The mathematical developments required to develop a computation tool based on such concepts are exposed. The case of viscous fluids (in the limit of the Newtonian fluid assumption<sup>2</sup>) has been particularly investigated, since it also allows the simulation of ideal fluids simply by setting the viscosity coefficients to zero. Many cases then are considered in order to illustrate the interest of the proposed approach, for instance, the attenuation of Rayleigh waves due to water damping, the sensitivity of Leaky waves to viscos-

ity, or the behavior of plate modes loaded on one side by viscous water. The corresponding theoretical results are discussed. The specific situation of pure shear waves as used in surface transverse waves (STWs) is particularly investigated. These waves are generally assumed poorly affected by water and other weakly viscous fluids. The limit of this hypothesis is examined theoretically.

## II. THEORY

### A. Modeling the acoustic behavior of ideal and viscous fluids

The theoretical representation of acoustic waves in fluids is usually performed using a pressure formulation. Nevertheless, in order to easily derive the corresponding Green's function, a displacement formulation can be constructed as well. For any fluid, the independent elastic constants required for such a formulation reduce to one, i.e.,  $C_{11}$  which is also equal to  $C_{12}$ , yielding  $C_{66}=0$  consequently. According to Ref. 2, a shear effect in a fluid between a moving solid and a reference solid results in a linear stress proportional to the velocity gradient via the coefficient  $\eta$  called shear viscosity or absolute viscosity of the fluid. In an isotropic homogeneous incompressible Newtonian fluid, the stress is proportional to the linear strain; this is called the Stokes law. In a very general approach,<sup>3</sup> one should also consider the compressive viscosity factor  $\zeta$ . The pressure in the fluid  $P$  is proportional to the displacement divergence via the fluid compressibility as

$$P = - \frac{1}{\chi} \frac{\partial u_i}{\partial x_i}. \quad (1)$$

In the proposed developments, we assume the absence of any relaxation phenomenon (no specific time dependence) within the considered fluids. The stress then can be written as

<sup>a)</sup>Electronic mail: ballandr@lpmo.edu

$$T_{ij} = - \left[ P + j\omega \left( \frac{2}{3} \eta - \zeta \right) S_{kk} \right] \delta_{ij} + 2j\omega \eta S_{ij}, \quad (2)$$

where  $T_{ij}$  and  $S_{ij}$  are the stress and strain tensors, respectively, and  $\omega$  is the angular frequency. One can remark that for  $\eta = \zeta = 0$  (no viscosity), Eq. (2) reduces to the classical pressure equilibrium with no shear effects ( $T_{ij} = 0$  for  $i \neq j$ ). According to the literature,<sup>4,5</sup> the compressive viscosity may be responsible for important effects and hence should in no way be neglected. For instance, in the case of water, the absolute viscosity equals 0.8 cP but the compressive viscosity is about 2.8 times larger.<sup>5</sup> These two numerical values are assumed in the numerical applications of Sec. III without any restriction and their respective influence on wave damping is evaluated.

## B. Fahmy-Adler formulation for viscous fluids

Let us now explain how one can represent the propagation of acoustic waves in viscous fluids as an eigenvector problem conformably to the general description of Fahmy-Adler<sup>6</sup> for solids. Without any loss of generality, one considers the propagation in the plane  $(x_1, x_3)$  and the dependence along  $x_2$  is given by the linear system to be solved, as shown further. We assume a harmonic dependence in time, with the implicit term  $e^{j\omega t}$  omitted. We define the following state vector, mixing displacement, and stress components in the propagation plane,

$$\mathbf{h} = \left\langle \begin{array}{ccc} \frac{T_{21}}{-j\omega} & \frac{T_{22}}{-j\omega} & \frac{T_{23}}{-j\omega} \\ u_1 & u_2 & u_3 \end{array} \right\rangle. \quad (3)$$

In a more general approach, one should add the electrical potential and the electrical displacement vector component along  $x_2$ , enabling one to represent the dielectric viscous fluids. For the sake of simplicity, we only focus on the acoustic contribution. The propagation equations provide the first derivatives of the in-plane stresses versus  $x_2$  as follows, using the notation  $\sigma_{ij} = T_{ij}/(-j\omega)$ ,

$$\frac{\partial}{\partial x_2} \begin{Bmatrix} \sigma_{21} \\ \sigma_{22} \\ \sigma_{23} \end{Bmatrix} = j\rho\omega [I] \begin{Bmatrix} u_1 \\ u_2 \\ u_3 \end{Bmatrix} - \frac{\partial}{\partial x_1} \begin{Bmatrix} \sigma_{11} \\ \sigma_{12} \\ \sigma_{13} \end{Bmatrix} - \frac{\partial}{\partial x_3} \begin{Bmatrix} \sigma_{31} \\ \sigma_{32} \\ \sigma_{33} \end{Bmatrix}. \quad (4)$$

We need three more equations to establish the first derivatives of the displacement versus  $x_2$ . This is performed by developing (2) as follows:

$$\begin{Bmatrix} \sigma_{11} \\ \sigma_{12} \\ \sigma_{13} \end{Bmatrix} = \frac{\partial}{\partial x_1} [A_{11}] \begin{Bmatrix} u_1 \\ u_2 \\ u_3 \end{Bmatrix} + \frac{\partial}{\partial x_2} [A_{12}] \begin{Bmatrix} u_1 \\ u_2 \\ u_3 \end{Bmatrix} + \frac{\partial}{\partial x_3} [A_{13}] \begin{Bmatrix} u_1 \\ u_2 \\ u_3 \end{Bmatrix},$$

$$\begin{Bmatrix} \sigma_{21} \\ \sigma_{22} \\ \sigma_{23} \end{Bmatrix} = \frac{\partial}{\partial x_1} [A_{12}] \begin{Bmatrix} u_1 \\ u_2 \\ u_3 \end{Bmatrix} + \frac{\partial}{\partial x_2} [A_{22}] \begin{Bmatrix} u_1 \\ u_2 \\ u_3 \end{Bmatrix} + \frac{\partial}{\partial x_3} [A_{23}] \begin{Bmatrix} u_1 \\ u_2 \\ u_3 \end{Bmatrix}, \quad (5)$$

$$\begin{Bmatrix} \sigma_{31} \\ \sigma_{32} \\ \sigma_{33} \end{Bmatrix} = \frac{\partial}{\partial x_1} [A_{13}] \begin{Bmatrix} u_1 \\ u_2 \\ u_3 \end{Bmatrix} + \frac{\partial}{\partial x_2} [A_{23}] \begin{Bmatrix} u_1 \\ u_2 \\ u_3 \end{Bmatrix} + \frac{\partial}{\partial x_3} [A_{33}] \begin{Bmatrix} u_1 \\ u_2 \\ u_3 \end{Bmatrix},$$

where matrices  $[A_{ij}]$  depend on the viscosity factors, the compressibility factor, and the frequency (see Appendix). From the second line of (5), one deduces the derivatives of the displacement versus  $x_2$ ,

$$\frac{\partial}{\partial x_2} \begin{Bmatrix} u_1 \\ u_2 \\ u_3 \end{Bmatrix} = [A_{22}]^{-1} \left( \begin{Bmatrix} \sigma_{21} \\ \sigma_{22} \\ \sigma_{23} \end{Bmatrix} - \frac{\partial}{\partial x_1} [A_{12}] \begin{Bmatrix} u_1 \\ u_2 \\ u_3 \end{Bmatrix} - \frac{\partial}{\partial x_3} [A_{23}] \begin{Bmatrix} u_1 \\ u_2 \\ u_3 \end{Bmatrix} \right). \quad (6)$$

Inserting (5) and (6) yields the following expressions of  $\sigma_{1j}$  and  $\sigma_{3j}$ :

$$\begin{Bmatrix} \sigma_{11} \\ \sigma_{12} \\ \sigma_{13} \end{Bmatrix} = \frac{\partial}{\partial x_1} [A_{11}] \begin{Bmatrix} u_1 \\ u_2 \\ u_3 \end{Bmatrix} + [A_{12}][A_{22}]^{-1} \left( \begin{Bmatrix} \sigma_{21} \\ \sigma_{22} \\ \sigma_{23} \end{Bmatrix} - \frac{\partial}{\partial x_1} [A_{12}] \begin{Bmatrix} u_1 \\ u_2 \\ u_3 \end{Bmatrix} - \frac{\partial}{\partial x_3} [A_{23}] \begin{Bmatrix} u_1 \\ u_2 \\ u_3 \end{Bmatrix} \right) + \frac{\partial}{\partial x_3} [A_{13}] \begin{Bmatrix} u_1 \\ u_2 \\ u_3 \end{Bmatrix}, \quad (7)$$

$$\begin{Bmatrix} \sigma_{31} \\ \sigma_{32} \\ \sigma_{33} \end{Bmatrix} = \frac{\partial}{\partial x_1} [A_{13}] \begin{Bmatrix} u_1 \\ u_2 \\ u_3 \end{Bmatrix} + [A_{23}][A_{22}]^{-1} \left( \begin{Bmatrix} \sigma_{21} \\ \sigma_{22} \\ \sigma_{23} \end{Bmatrix} - \frac{\partial}{\partial x_1} [A_{12}] \begin{Bmatrix} u_1 \\ u_2 \\ u_3 \end{Bmatrix} - \frac{\partial}{\partial x_3} [A_{23}] \begin{Bmatrix} u_1 \\ u_2 \\ u_3 \end{Bmatrix} \right) + \frac{\partial}{\partial x_3} [A_{33}] \begin{Bmatrix} u_1 \\ u_2 \\ u_3 \end{Bmatrix}.$$

The above system is related to the state vector  $\mathbf{h}$  as follows:

$$\begin{aligned}
\begin{Bmatrix} \sigma_{11} \\ \sigma_{12} \\ \sigma_{13} \end{Bmatrix} &= \begin{bmatrix} [A_{12}][A_{22}]^{-1} & [A_{12}][A_{22}]^{-1} \left( \frac{\partial}{\partial x_1} [A_{12}] + \frac{\partial}{\partial x_3} [A_{23}] \right) \\ \frac{\partial}{\partial x_1} [A_{11}] + \frac{\partial}{\partial x_3} [A_{13}] \end{bmatrix} \begin{Bmatrix} \sigma_{21} \\ \sigma_{22} \\ \sigma_{23} \\ u_1 \\ u_2 \\ u_3 \end{Bmatrix}, \\
\begin{Bmatrix} \sigma_{31} \\ \sigma_{32} \\ \sigma_{33} \end{Bmatrix} &= \begin{bmatrix} [A_{23}][A_{22}]^{-1} & -[A_{23}][A_{22}]^{-1} \left( \frac{\partial}{\partial x_1} [A_{12}] \right. \\ \left. + \frac{\partial}{\partial x_3} [A_{23}] \right) \\ \frac{\partial}{\partial x_1} [A_{13}] + \frac{\partial}{\partial x_3} [A_{33}] \end{bmatrix} \begin{Bmatrix} \sigma_{21} \\ \sigma_{22} \\ \sigma_{23} \\ u_1 \\ u_2 \\ u_3 \end{Bmatrix}.
\end{aligned} \tag{8}$$

Inserting (4) and (8), and combining the result with (6), we obtain the eigenvalue formulation we are looking for. Assuming a harmonic dependence of the fields versus  $x_1$  and  $x_3$ , replacing the corresponding gradients by  $-j\omega s_1$  and  $-j\omega s_3$  (with  $s_i$  the slowness along  $x_i$ ) yields

$$\begin{aligned}
\frac{\partial}{\partial x_2} \begin{Bmatrix} \sigma_{21} \\ \sigma_{22} \\ \sigma_{23} \\ u_1 \\ u_2 \\ u_3 \end{Bmatrix} &= \begin{bmatrix} [\alpha_{11}] & [\alpha_{12}] \\ [A_{22}]^{-1} & [A_{22}]^{-1} (j\omega s_1 [A_{12}] + j\omega s_3 [A_{23}]) \end{bmatrix} \\
&\times \begin{Bmatrix} \sigma_{21} \\ \sigma_{22} \\ \sigma_{23} \\ u_1 \\ u_2 \\ u_3 \end{Bmatrix},
\end{aligned} \tag{9}$$

with

$$\begin{aligned}
[\alpha_{11}] &= [(j\omega s_1 [A_{12}] + j\omega s_3 [A_{23}])[A_{22}]^{-1}] \\
[\alpha_{12}] &= \{j\omega \rho [I] + j\omega s_1 [[A_{12}][A_{22}]^{-1} (j\omega s_1 [A_{12}] \\
&\quad + j\omega s_3 [A_{23}]) - j\omega (s_1 [A_{11}] + s_3 [A_{13}])] \\
&\quad + j\omega s_3 [[A_{23}][A_{22}]^{-1} (j\omega s_1 [A_{12}] + j\omega s_3 [A_{23}]) \\
&\quad - j\omega (s_1 [A_{13}] + s_3 [A_{33}])]\}.
\end{aligned}$$

The main difficulty introduced by the proposed development

consists in the frequency dependence of the matrices  $[A_{ij}]$ , requiring their computation for each frequency point.

### C. Green's function of viscous fluids

The way the above relations can be used to compute Green's function of the medium is detailed in Refs. 7 and 8. Only a brief description of its derivation is reported here. Conformably to the Fahmy-Adler approach,<sup>6</sup> one considers the above-defined state vector  $\mathbf{h}$  to describe the acoustic properties of a semi-infinite or finite thickness medium potentially inserted in a stack of layers with assumed flat interfaces. For a given surface slowness  $(s_1, s_3)$ ,  $\mathbf{h}$  can be represented as the product of a matrix  $\mathbf{F}$  composed of the eight eigenvectors of the considered medium with a diagonal matrix  $\Delta(x_2)$  of rank  $8 \times 8$ , which describes the dependence of the acoustic field versus  $x_2$  via the eigenvalues  $s_2$ , and with a vector  $\mathbf{a}$  accounting for the amplitudes of the partial waves,

$$\mathbf{h}(x_2) = \mathbf{F}\Delta(x_2)\mathbf{a} \exp[j\omega(t - s_1 x_1 - s_3 x_3)]. \tag{10}$$

For viscous fluids, the matrices  $\mathbf{F}$  depend on frequency (contrarily to ideal fluids and classical solids). As in Refs. 7–9, we introduce the vector variable  $\mathbf{g}^{(m)}$  which is split in two parts to differentiate between the incident  $[\mathbf{g}^{(m-)}]$  and reflected  $[\mathbf{g}^{(m+)}]$  waves defined as follows:

$$\mathbf{g}^{(m-)}(X_{m-1}) = \mathbf{R}^{(m)}\mathbf{g}^{(m+)}(X_{m-1}), \tag{11}$$

where  $m$  is the number of the considered layer in the stack ( $m=1$  for semi-infinite media) and  $\mathbf{R}^{(m)}$  is a reflection matrix relating the incident and reflected partial waves. The reflection matrices of each interface of the stack are then recursively deduced from the reflection matrix at the first interface.<sup>8,9</sup> This is achieved by introducing two submatrices  $\mathbf{K}$  and  $\mathbf{L}$ , respectively, associated with the reflected and incident partial waves,

$$[\mathbf{F}^{(m+1)}]^{-1}\mathbf{F}^{(m)} \begin{bmatrix} I_4 \\ \Delta^{(m-)}(-t_m)\mathbf{R}^{(m)}\Delta^{(m+)}(t_m) \end{bmatrix} = \begin{pmatrix} \mathbf{K} \\ \mathbf{L} \end{pmatrix}, \tag{12}$$

with  $t_m$  the thickness of the  $m$ th layer of the stack. These matrices are used to compute the reflection matrix of the  $(m+1)$  layer:  $\mathbf{R}^{(m+1)} = \mathbf{L}\mathbf{K}^{-1}$ . This recursive scheme is repeated until the top layer of the stack (numbered  $M$ ) is reached, at which surface we intend to compute Green's function. The state vector  $\mathbf{h}$  then reads

$$\begin{aligned}
\mathbf{h}(X_M) &= \mathbf{F}^{(M)}\mathbf{g}^{(M)}(X_M) = \mathbf{F}^{(M)}[\Delta^{(M-)}(-t_M)\mathbf{R}^{(M)}\Delta^{(M+)} \\
&\quad \times (t_M)]\mathbf{g}^{(M+)}(X_M) = \begin{pmatrix} \mathbf{N} \\ \mathbf{P} \end{pmatrix}\mathbf{g}^{(M+)}(X_M).
\end{aligned} \tag{13}$$

In (13), we have defined two submatrices  $\mathbf{N}$  and  $\mathbf{P}$ , respectively, associated with the displacement field and the stresses. Green's function which relates  $u_i$  to  $T_{2j}$  then is directly given by the product  $\mathbf{G} = \mathbf{N}\mathbf{P}^{-1}$ . As in Ref. 10, we intend to compute Green's function at the interface between two media. Since  $\mathbf{G}$  can be computed following the above procedure at any surface or interface of a given material stack (still assuming flat parallel interfaces), it can be derived for any configurations (e.g., semi-infinite piezoelectric solids, plates, or a layered waveguide in contact with viscous fluids in our

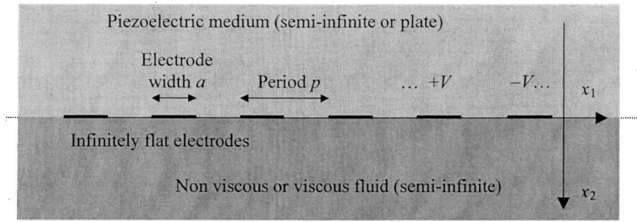


FIG. 1. Scheme of the typical geometry considered for simulations.

case). In the case of a semi-infinite substrate in contact with a semi-infinite viscous fluid, Green's function at the interface between the two media depends on the frequency in a complicated way (due to viscosity effects). It is then computed for each frequency point as in the case of dispersive waveguides. Note that in the spectral domain, Green's function relates the generalized displacements  $u_i$  (Refs. 7–9) (including the potential  $\phi$  as  $u_4$ ) and the generalized surface stresses  $T_{2j}$  (where  $T_{24}=D_2$  the electrical displacement normal to the surface) as  $u_i=G_{ij}T_{2j}$ .

#### D. Blötekjaër's harmonic admittance

Green's function can be used to compute the actual response of infinitely periodic-guided elastic wave devices using different approaches.<sup>9–11</sup> In this work, we derive the celebrated effective permittivity<sup>12</sup> from Green's function as follows:

$$\varepsilon_{\text{EFF}}(\omega, s_1) = \frac{1}{j|s|G_{44}(\omega, s_1)}, \quad (14)$$

yielding a frequency-dependent effective permittivity. In (14), the expression of  $\varepsilon_{\text{EFF}}$  is restricted to the sagittal plane in which the waves are excited, assuming an infinite aperture of the transducer along  $x_3$  ( $s_3$  then is set to zero). It is used to compute a harmonic admittance,<sup>12</sup> neglecting the mechanical contribution of the electrodes. This approach first used in Ref. 11 for interface wave computations enables one to simulate the excitation of acoustic waves by nonmassive infinite periodic transducers (interdigital transducers (IDT), for instance) at any interface of any layered structure. In this section, we just point out the way the above effective permittivity is introduced in the calculation. The potential  $\phi$  and electrical charge  $Q$  are developed as Bloch-Floquet series to meet the periodic conditions (see Fig. 1 for axis definition) as follows:

$$\begin{aligned} \phi &= \sum_{n=-\infty}^{+\infty} \tilde{\phi}_n e^{-j\omega s_n x_1}, \\ Q &= \sum_{n=-\infty}^{+\infty} \tilde{q}_n e^{-j\omega s_n x_1}, \end{aligned} \quad (15)$$

where  $s_n = s_1 + 2\pi n / (p\omega)$  is the equivalent slowness of the  $n$ th term of the series. The relation between the weights of  $\phi$  and  $Q$  is established in the spectral domain conformably to the effective permittivity definition<sup>12</sup> as follows:

$$\tilde{q}_n = \omega |s_n| \varepsilon_n \tilde{\phi}_n \quad \text{with } \varepsilon_n = \varepsilon_{\text{EFF}}(s_n). \quad (16)$$

The boundary conditions of the addressed problem consist in the absence of charge between the electrodes and the nullity of the electrical field parallel to the excitation surface under the electrodes. The corresponding equations are solved thanks to a Legendre-polynomial development of the unknown fields.<sup>12</sup> The weights of this development are related to the potential and charge coefficients as follows:

$$\begin{aligned} \omega s_n \tilde{\phi}_n &= \sum_{m=M_1}^{M_2} \alpha_m \text{sgn}(m-n) P_{n-m} \left[ \cos\left(\frac{\pi a}{p}\right) \right], \\ \tilde{q}_n &= \sum_{m=M_1}^{M_2} \beta_m P_{n-m} \left[ \cos\left(\frac{\pi a}{p}\right) \right], \end{aligned} \quad (17)$$

where  $P_n$  is the  $n$ th Legendre polynomial,  $a$  is the width of the electrode, and  $p$  the grating period. The weights of the Legendre developments  $\alpha_m$  and  $\beta_m$  then become the actual unknowns of the problem.  $M_1$  and  $M_2$  are the bounds of the discrete summation in (17), theoretically equal to  $-\infty$  and  $+\infty$ . Practically, infinite sums cannot be handled for computation and the summations of (15) and (17) have to be truncated [ $N_1$  and  $N_2$  represent the finite bounds of the sum in (15)]. For a given value of  $\omega$ , the effective permittivity is known to converge towards an asymptotic value written,  $\varepsilon_\infty$ . This is correct for usual materials, but a particular care must be paid to the case of viscous fluids, for which the frequency is intricately related to the intermediate matrix  $[A_{ij}]$  used to derive Green's function. However, for usual frequencies (smaller than 10 GHz), it is possible to find a slowness large enough to allow for a satisfying definition of  $\varepsilon_\infty$  (i.e., for which the latter value is moderately affected by the frequency). By properly choosing the values of  $(M_1, M_2)$  and  $(N_1, N_2)$ ,<sup>12</sup> one can establish the following relation between  $\alpha_m$  and  $\beta_m$ :

$$\text{sgn}(n)\beta_m = \varepsilon_\infty \text{sgn}(n-m)\alpha_m. \quad (18)$$

Combining (17) and (18) yields the following homogeneous algebraic system which must be solved in our case for each frequency point of the development:

$$\left\{ \left[ \text{sgn}(n-m) - \frac{\varepsilon_\infty}{\varepsilon_n} \text{sgn}(n) \right] P_{n-m} \left[ \cos\left(\frac{\pi a}{p}\right) \right] \right\} \{\alpha_m\} = 0. \quad (19)$$

Once the coefficients are derived from (19), the computation of the harmonic potential  $V_{\text{harm}}$  and current  $I_{\text{harm}}$  is performed as described in Ref. 12, yielding the definition of the harmonic admittance as the ratio of  $I_{\text{harm}}$  over  $V_{\text{harm}}$ . The computation of this value allows for the identification of coupled acoustic waves generated by nonmassive IDTs and their characterization (phase velocity, coupling strength, propagation loss, and reflection coefficient). In the next section, we consider numerous examples for which the influence of viscous fluids on different waveguides is analyzed.

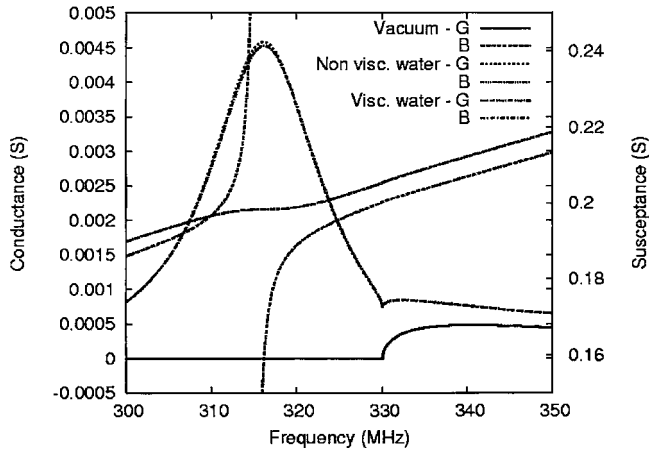


FIG. 2. Harmonic admittance of an infinite periodic IDT on  $(YXl)/36^\circ$  cut of quartz with an adjacent semi-infinite fluid domain, influence on the Rayleigh, and surface skimming bulk wave (SSBW) signature (period  $5 \mu\text{m}$ , metallization ratio  $a/p=0.5$ ).

### III. COMPUTATION RESULTS

Calculations have been performed for different kinds of wave polarization on the most used piezoelectric substrates, i.e., quartz, lithium tantalate, and lithium niobate, assuming a semi-infinite dielectric fluid domain (water) adjacent to the solid substrate. An isotropic dielectric constant equal to  $10 \text{ pF/m}$  was arbitrarily set for the fluid. This explains the change in static capacitance when passing from vacuum to the fluid load on the following admittance plots. The absolute viscosity of water [close to  $1 \text{ cP}$  (Ref. 8)] was changed from  $1$  to  $10 \text{ cP}$  and  $100 \text{ cP}$  to check its influence on the wave characteristics. For all tested materials, Rayleigh as well as leaky SAW have been considered. For quartz, surface transverse waves also have been taken into account. Finally, the influence of a water load on acoustic plate modes (APMs) on  $(YXl)/36^\circ$  cut of quartz has been simulated for both viscous and nonviscous water. Note that all the admittance results are given for a unit width aperture.

Figure 1 shows the general geometry of the problem. For the sake of consistence, a metal ratio equal to  $0.5$  was considered for all computations, and the period was fixed to  $5 \mu\text{m}$  (acoustic wavelength forced to  $10 \mu\text{m}$ ). Figures 2 and 3 show the results obtained for the  $(YXl)/36^\circ$  cut of quartz, expended in three sections to magnify the different contributions to the harmonic admittance.

The damping of Rayleigh wave by the water load is clearly shown in Fig. 2. Also an influence is pointed out on the surface skimming bulk wave (SSBW) close to the Rayleigh wave and radiated from the surface, mainly due to the damped Rayleigh wave conductance. The very small influence of viscosity on the Rayleigh wave signature yields almost no difference between the viscous and nonviscous water-loaded admittances which indicates that the main leakage source of the propagation is due to the acoustic radiation in the fluid.

Figures 3(a) and 3(b) show the influence of a water load on the two leaky modes (fast shear and longitudinal) on  $(YXl)/36^\circ$  cut of quartz, which is clearly less dramatic than in the case of the Rayleigh wave. These two modes partially

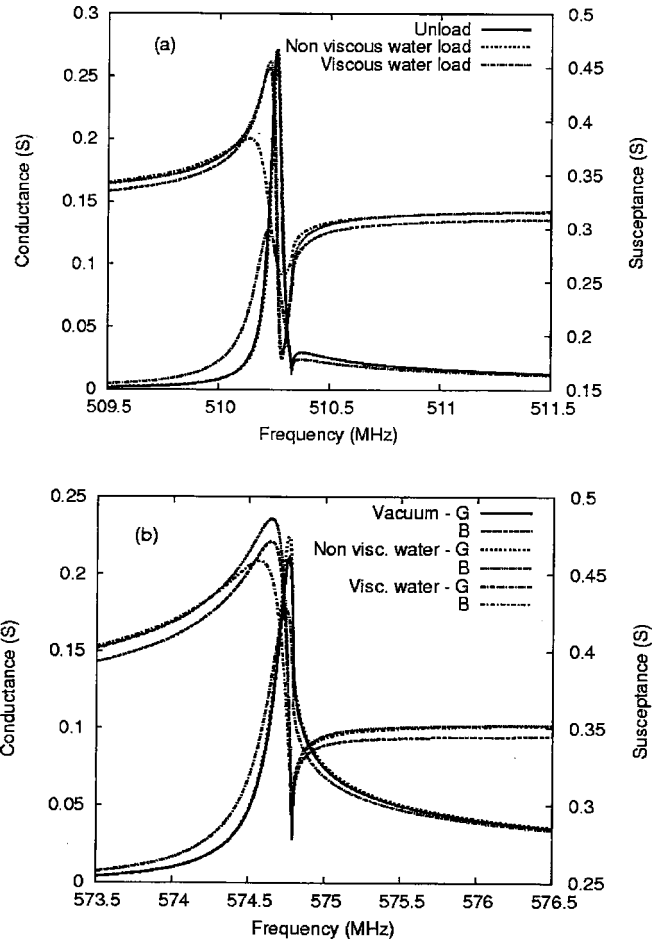


FIG. 3. Harmonic admittance of an infinite periodic IDT on  $(YXl)/36^\circ$  cut of quartz with vacuum, ideal and viscous water as adjacent semi-infinite media, and (a) shear and (b) longitudinal-radiated bulk waves (period  $5 \mu\text{m}$ , metallization ratio  $a/p=0.5$ ).

guided by the surface exhibit an almost pure polarization and then a negligible component normal to the surface. This means that they radiate almost no energy in the fluid. However, they are affected by viscosity effects, yielding a significant increase of losses due to viscous shearing within the fluid. This is particularly emphasized for the fast shear leaky wave which is almost not affected by the presence of ideal water. In contact with viscous water, the conductance of this mode is reduced by more than a factor of 2 and the quality factor of the mode changes from  $8300$  to  $3200$ . (This value is derived from the conductance peak relative to the mode as the ratio of its central frequency divided by its width at half height.) In that particular case, the impact of rather small viscosity properties at usual frequencies cannot be neglected. One can note that the central frequency is also slightly shifted down. A more surprising result is the robustness of the longitudinal mode in contact with water. In that case, the mode guiding even seems improved according to the slight increase of the corresponding conductance peak. However, viscosity effects also dramatically reduce its excitation efficiency. Again in that case, they induce a slight frequency decrease of the mode. The values of the quality factor for the different analyzed operating conditions are, respectively,  $2650$  (vacuum),  $3000$  (ideal water), and  $1850$  (viscous water).

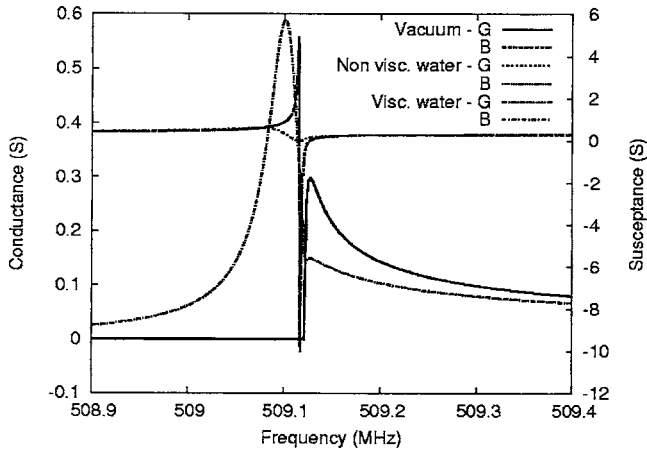


FIG. 4. Harmonic admittance of an infinite periodic IDT on  $(YXl)/36^\circ/90^\circ$  cut of quartz (STW cut) with vacuum, and ideal and viscous water as adjacent semi-infinite media (period  $5\ \mu\text{m}$ , metallization ratio  $a/p=0.5$ ).

Figure 4 shows the same computations performed for STW on the  $(YXl)/36^\circ/90^\circ$  quartz cut. The curves relative to vacuum and to nonviscous water as adjacent media are confound, since no shear displacement can develop in perfect fluids. As soon as viscosity is introduced, the STW is dramatically damped, yielding a quality factor of 12 400 which rapidly falls down when increasing the viscosity, as shown in Fig. 5. A quality factor of 2000 is predicted for a viscosity equal to 10 cP and it passes under 500 when increasing the viscosity to 100 cP. This is an important issue to consider when expecting using the STW for immersed biomedical applications, since biological liquids may exhibit rather large viscosity values.

The case of Love waves is also investigated to check whether the elimination of propagation loss associated with the STW allows for improving the device operation. In that purpose, we assume a silica overlay atop the quartz substrate to guide the pure shear wave. The electric excitation is assumed at the interface between the quartz substrate and the silica overlay. The thickness of the  $\text{SiO}_2$  layer was arbitrarily set to 500 nm, yielding a Love wave propagating with a

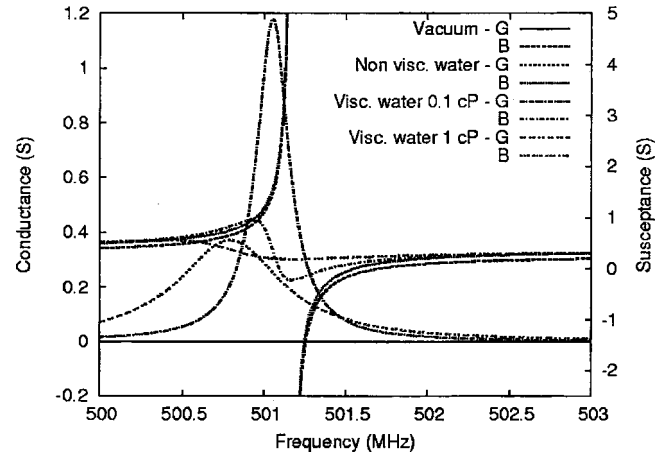


FIG. 6. Harmonic admittance of an infinite periodic IDT at the interface between a 500-nm-thick  $\text{SiO}_2$  overlay and the  $(YXl)/36^\circ/90^\circ$  cut of quartz (excitation of Love waves) with vacuum, and ideal and viscous water (0.1 and 1 cP) as adjacent semi-infinite media (period  $5\ \mu\text{m}$ , metallization ratio  $a/p=0.5$ , and 500-nm-thick silica overlay).

phase velocity close to  $5010\ \text{m s}^{-1}$  with a coupling coefficient [the usual  $K_s^2$  (Ref. 1)] equal to 2.1%. As previously, a water load does not significantly change the harmonic admittance of the structure. However, viscosity effects again yield a dramatic reduction of the wave conductance, which then presents a finite quality factor. Note that for a 0.1 cP viscosity, this factor equals 2100 but it falls down to 660 for 1 cP (standard water). We also point out a frequency shift of about 250 kHz between these two operating conditions. Love waves on quartz, consequently, are very sensitive to viscosity and seem hardly capable to operate with highly viscous fluids (viscosity larger than 50 cP) as the loading medium (Fig. 6).

Regarding these results, it then sounds interesting to analyze the robustness of longitudinally polarized waves in the presence of fluids exhibiting such viscosities. In that view, we have considered the case of  $(YZ)$ -cut lithium niobate, on which a well-coupled Rayleigh wave can propagate but also a high velocity longitudinal wave may be trapped under thick

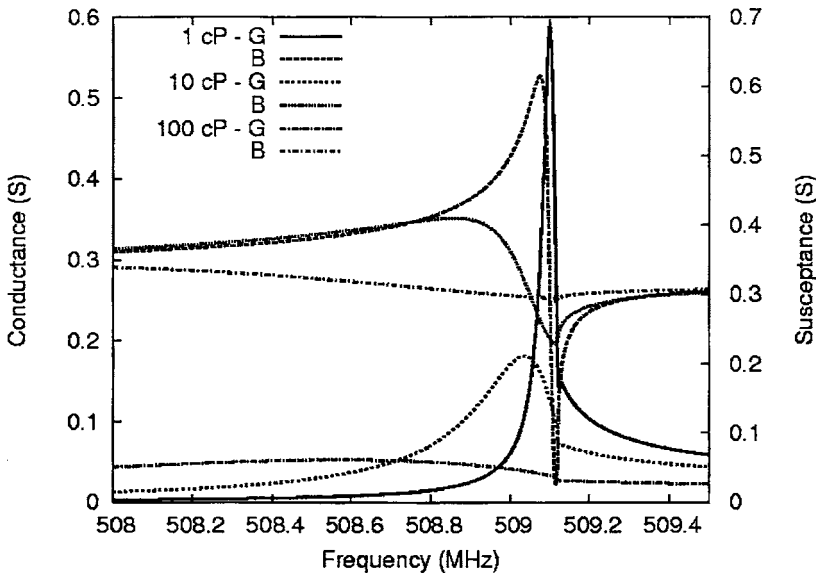


FIG. 5. Influence of the viscosity on the STW response on  $(YXl)/36^\circ/90^\circ$  quartz—absolute viscosities equal to 1, 10, and 100 cP (compressive viscosity equals 2.8 times the absolute one).

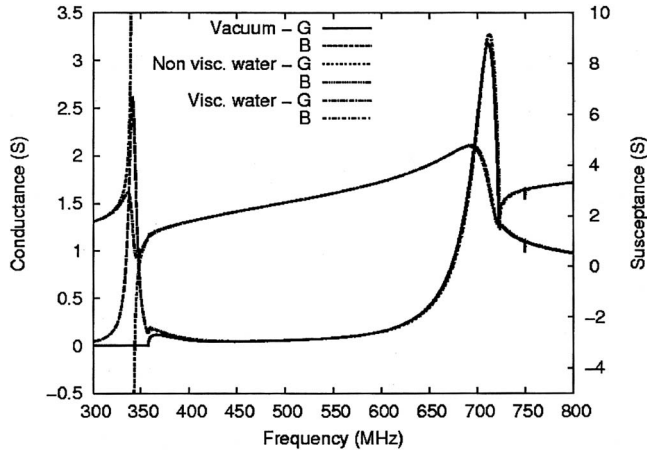


FIG. 7. Harmonic admittance of an infinite periodic IDT on (YZ) cut of LiNbO<sub>3</sub> with vacuum, and ideal and viscous water as adjacent semi-infinite media (period 5 μm, metallization ratio  $a/p=0.5$ ).

electrodes. Even if we cannot simulate such an electrode configuration, we can point out the longitudinal wave signature on the harmonic admittance and then predict the influence of viscous fluids on this kind of wave. Figure 7 shows the influence of ideal and viscous water loads on the harmonic admittance signatures of the Rayleigh and longitudinal waves on (YZ)LiNbO<sub>3</sub> cut. We also have reported the evolution of these responses for various values of viscosity in Fig. 8, which shows that the longitudinal wave is clearly less affected by viscosity than shear waves on quartz area. One could also argue that the Rayleigh wave signature does not change when increasing the viscosity, but it should be kept in mind that this wave almost vanishes when loaded by water, whereas the amplitude of the longitudinal wave almost remains unchanged for the different considered operating conditions.

However, such a longitudinal wave cannot be considered as a relevant demonstration of interest for immersed applications since its signature on the harmonic admittance remains weak compared to a real surface-guided mode. We then investigate the operation of Lamb waves loaded by fluids. This is a very interesting configuration in which very thin plates

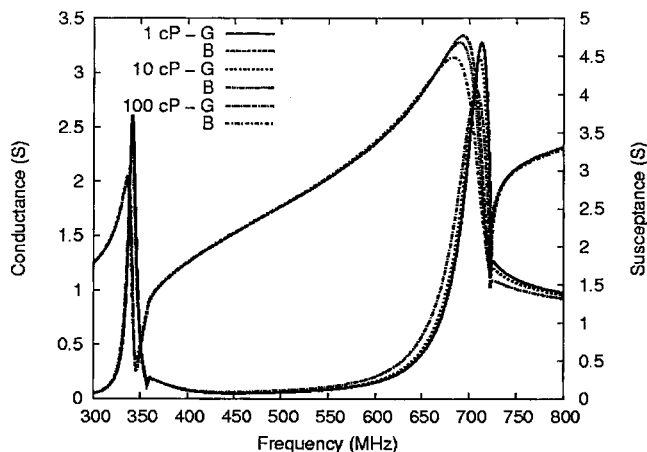


FIG. 8. Influence of the viscosity on the Rayleigh wave and longitudinal wave responses on (YZ)LiNbO<sub>3</sub>—absolute viscosities equal to 1, 10, and 100 cP (compressive viscosity equals 2.8 times the absolute one).

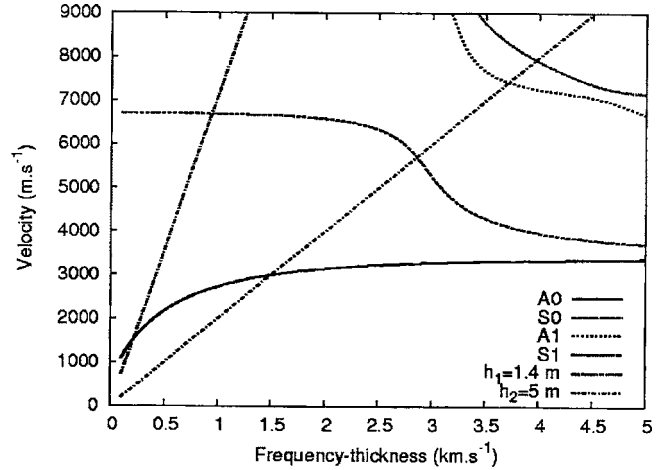


FIG. 9. Velocity curves of Lamb waves on a (YZ) lithium niobate thin plate. The straight lines plotted on this graph correspond to plate thicknesses  $h_1=1.4 \mu\text{m}$  and  $h_2=5 \mu\text{m}$  considered for the following computations. Their intersections with the velocity curves indicate the actual velocities of the excited Lamb modes.

simultaneously can support waves not damped by the water load because of their very small phase velocity (lower than  $1500 \text{ m s}^{-1}$ ) and also high velocity waves that almost behave like pure longitudinal modes. Figure 9 shows the dispersion curves of Lamb waves on a (YZ)LiNbO<sub>3</sub> cut plate. For thickness-frequency products smaller than  $220 \text{ m s}^{-1}$ , the first antisymmetric mode  $A_0$  exhibits a phase velocity smaller than the one of water and one can also remark that the first symmetric mode ( $S_0$ ) velocity is almost constant and close to the longitudinal bulk wave velocity (about  $7000 \text{ m s}^{-1}$ ). Note that for the considered wavelength, the polarization of this mode principally lies along the  $x$  axis. (The elliptic polarization actually is very weak in that case.)

We check the behavior of such a device for two plate thicknesses, i.e. 1.4 and 5 μm. A simple geometric construction gives the operating frequencies for each excited Lamb mode. For a plate thickness  $h$ , the slope  $m$  of a straight line passing through the origin is equal to the wavelength-plate thickness ratio ( $m=\lambda/h$ ). For the imposed wavelength ( $\lambda=10 \mu\text{m}$ ), the slopes are, respectively,  $m_1=7.14$  and  $m_2=2$  for thicknesses  $h_1=1.4 \mu\text{m}$  and  $h_2=5 \mu\text{m}$ . In the first case, the  $A_0$  mode is close to the velocity threshold at which the mode radiates its energy in water. However, due to the water mass loading, its contribution to the harmonic admittance is shifted down, yielding no leakage due to radiation in water [see Fig. 10(a)]. Its electromechanical coupling is very weak but one should note that such a structure (a single-crystal plate, symmetric around its neutral line) is poorly adapted to excite antisymmetric waves. On the other hand, a coupling factor of more than 4% is obtained for the  $S_0$  mode. Figure 10(a) shows the degradation of the  $A_0$  mode amplitude when increasing the viscosity. An identical behavior is pointed out for the  $S_0$  mode which is damped by water but still exhibits a well-defined response [Fig. 10(b)]. The mode amplitude dramatically falls down for values of viscosity larger or equal to 10 cP, but the  $A_0$  mode actually exhibits a sharper peak than the  $S_0$  does under these operating conditions. In that case, one can point out that the main issue is to efficiently excite

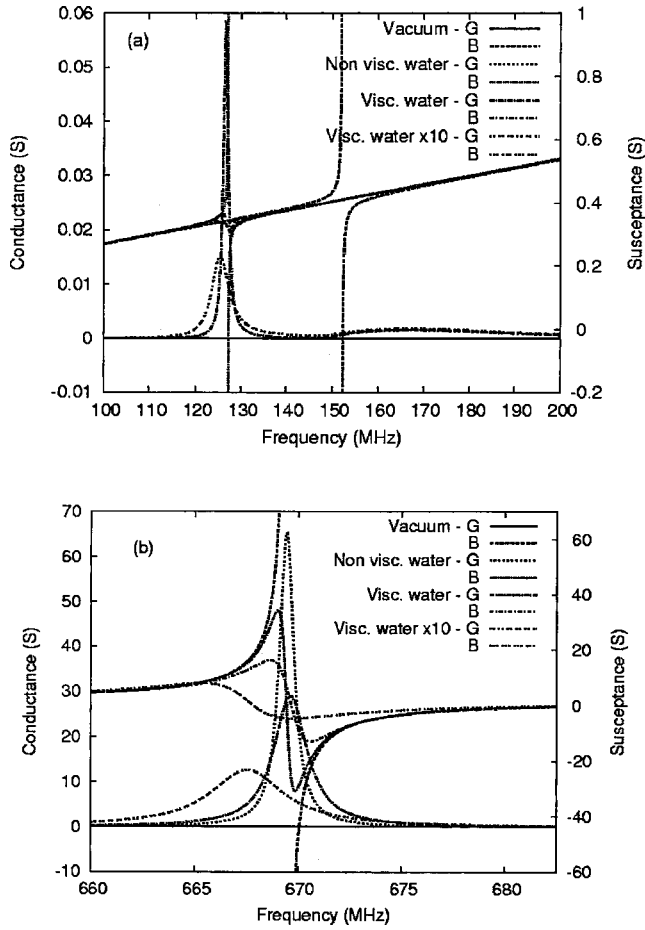


FIG. 10. Harmonic admittance of an infinite periodic IDT on a 1.4- $\mu\text{m}$ -thick plate of  $\text{LiNbO}_3(\text{YZ})$  cut with vacuum, and ideal and viscous water (1 and 10 cP, compressive viscosity equals 2.8 times the absolute one) as adjacent semi-infinite media. (a)  $A_0$  mode and (b)  $S_0$  mode (period 5  $\mu\text{m}$ , metallization ratio  $a/p=0.5$ ).

the  $A_0$  mode for any exploitation of its properties. A bimorph structure (naturally nonsymmetric) would certainly help in that purpose.

For the 5- $\mu\text{m}$ -thick plate, the situation is quite different, since the  $A_0$  mode is largely above the radiation threshold, and the  $A_1$  and  $S_1$  modes do contribute now to the harmonic admittance (see Fig. 9). The same computations as previously performed are then conducted for that case. The  $A_0$  and  $S_0$  modes almost vanish as soon as the plate is loaded by water [Fig. 11(a)]. However, the  $A_1$  mode exhibit more robustness to the presence of water, as shown in Fig. 11(b). It still exhibits a well-defined peak on the conductance even for 10 cP viscosity. This result tends to prove that high-order Lamb modes could operate as well as the low velocity  $A_0$  mode even when submitted to a water load. This presents the advantage of an efficient excitation together with a device architecture simpler than the one required for the exploitation of the  $A_0$  mode (very thin bimorph structures).

#### IV. CONCLUSION

A model describing the propagation of acoustic waves in fluids exhibiting or not exhibiting viscosity properties has been developed and implemented. The use of a harmonic admittance enables one to determine the influence of nonvis-

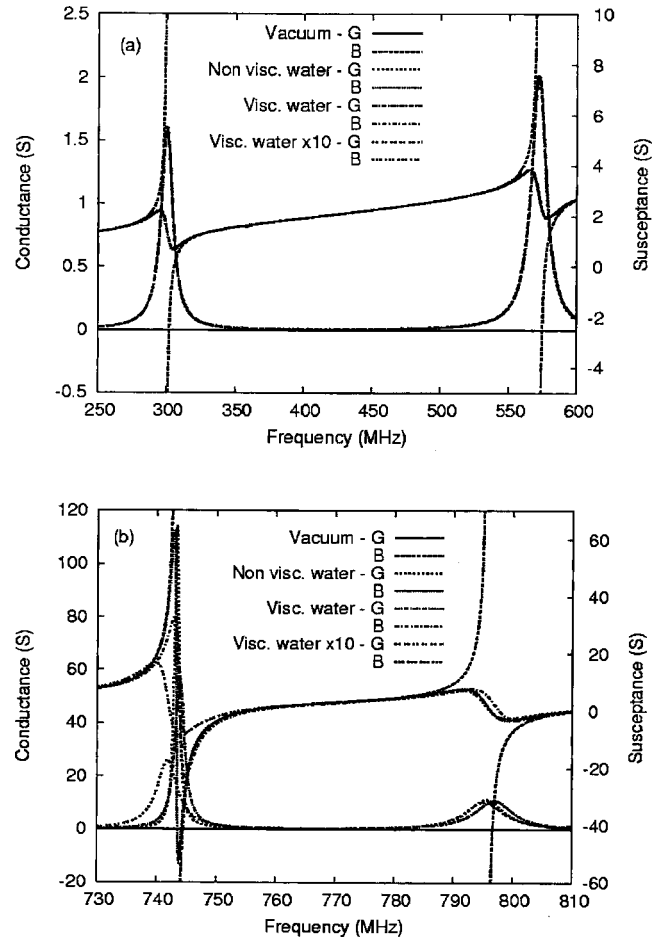


FIG. 11. Harmonic admittance of an infinite periodic IDT on a 5- $\mu\text{m}$ -thick plate of  $\text{LiNbO}_3(\text{YZ})$  cut with vacuum, ideal and viscous water (1 and 10 cP, compressive viscosity equals 2.8 times the absolute one) as adjacent semi-infinite media. (a)  $A_0$  and  $S_0$  modes and (b)  $A_1$  and  $S_1$  modes (period 5  $\mu\text{m}$ , metallization ratio  $a/p=0.5$ ).

cous and viscous water loads on various combinations of waves/substrates. The damping of Rayleigh wave due to the radiation of the displacement field component normal to the guiding surface is clearly pointed out. It is also shown that waves exhibiting a quasipure shear polarization are almost not affected by the presence of water. However, the influence of viscosity appears even for pure shear waves on quartz, yielding an additional leakage phenomenon generally neglected for practical applications. A more unusual result is the robustness of longitudinally polarized waves versus the presence of water. Moreover, according to our computations, since no shear effect is involved in this kind of propagation, longitudinal modes or pseudomodes would be less sensitive to viscosity than shear waves. Also Lamb waves were tested, showing the interest of the  $A_0$  mode on very thin plates but also the capability of higher-order modes to operate even with moderately viscous water loads.

These results suggest that contrarily to what is usually admitted (i.e., only pure shear wave and modes with a velocity smaller than the water threshold—1500  $\text{m s}^{-1}$ —can be operated in viscous fluids), different kind of waves and modes can be exploited for immersed application even with moderately viscous fluids. This means there are still a lot of opportunities to point out the optimal combinations of mate-

rials, wave natures, and electrode structures for the development of electroacoustic devices operating in contact with fluids (for instance, in sensing applications within organic bodies).

In this context, the simulation of more complicated electrode structures using a combination of finite element analysis boundary element methods would yield better insights and new ideas in the development of such devices.

## ACKNOWLEDGMENTS

Special thanks are due to J. B. Briot, Th. Pastureaud, R. Lardat, and W. Steichen for fruitful discussions.

## APPENDIX: DEFINITION OF THE MATRICES $[A_{IJ}]$

We express the stress field according to (2) to define the matrices that appear in (5) as follows:

$$\begin{aligned}
 \begin{Bmatrix} T_{11} \\ T_{12} \\ T_{13} \end{Bmatrix} &= \frac{\partial}{\partial x_1} \begin{bmatrix} \frac{1}{\chi} + j(\frac{4}{3}\eta + \zeta)\omega & 0 & 0 \\ 0 & j\omega\eta & 0 \\ 0 & 0 & j\omega\eta \end{bmatrix} \begin{Bmatrix} u_1 \\ u_2 \\ u_3 \end{Bmatrix} \\
 &+ \frac{\partial}{\partial x_2} \begin{bmatrix} 0 & \frac{1}{\chi} - j(\frac{2}{3}\eta - \zeta)\omega & 0 \\ j\omega\eta & 0 & 0 \\ 0 & 0 & 0 \end{bmatrix} \begin{Bmatrix} u_1 \\ u_2 \\ u_3 \end{Bmatrix} \\
 &+ \frac{\partial}{\partial x_3} \begin{bmatrix} 0 & 0 & \frac{1}{\chi} - j(\frac{2}{3}\eta - \zeta)\omega \\ 0 & 0 & 0 \\ j\omega\eta & 0 & 0 \end{bmatrix} \begin{Bmatrix} u_1 \\ u_2 \\ u_3 \end{Bmatrix}, \\
 \begin{Bmatrix} T_{21} \\ T_{22} \\ T_{23} \end{Bmatrix} &= \frac{\partial}{\partial x_1} \begin{bmatrix} 0 & j\omega\eta & 0 \\ \frac{1}{\chi} - j(\frac{2}{3}\eta - \zeta)\omega & 0 & 0 \\ 0 & 0 & 0 \end{bmatrix} \begin{Bmatrix} u_1 \\ u_2 \\ u_3 \end{Bmatrix} \\
 &+ \frac{\partial}{\partial x_2} \begin{bmatrix} j\omega\eta & 0 & 0 \\ 0 & \frac{1}{\chi} + j(\frac{4}{3}\eta + \zeta)\omega & 0 \\ 0 & 0 & j\omega\eta \end{bmatrix} \begin{Bmatrix} u_1 \\ u_2 \\ u_3 \end{Bmatrix} \\
 &+ \frac{\partial}{\partial x_3} \begin{bmatrix} 0 & 0 & 0 \\ 0 & 0 & \frac{1}{\chi} - j(\frac{2}{3}\eta - \zeta)\omega \\ 0 & j\omega\eta & 0 \end{bmatrix} \begin{Bmatrix} u_1 \\ u_2 \\ u_3 \end{Bmatrix}, \quad (A1) \\
 \begin{Bmatrix} T_{31} \\ T_{32} \\ T_{33} \end{Bmatrix} &= \frac{\partial}{\partial x_1} \begin{bmatrix} 0 & 0 & j\omega\eta \\ 0 & 0 & 0 \\ \frac{1}{\chi} - j(\frac{2}{3}\eta - \zeta)\omega & 0 & 0 \end{bmatrix} \begin{Bmatrix} u_1 \\ u_2 \\ u_3 \end{Bmatrix} \\
 &+ \frac{\partial}{\partial x_2} \begin{bmatrix} 0 & 0 & 0 \\ 0 & 0 & j\omega\eta \\ 0 & \frac{1}{\chi} - j(\frac{2}{3}\eta - \zeta)\omega & 0 \end{bmatrix} \begin{Bmatrix} u_1 \\ u_2 \\ u_3 \end{Bmatrix} \\
 &+ \frac{\partial}{\partial x_3} \begin{bmatrix} j\omega\eta & 0 & 0 \\ 0 & j\omega\eta & 0 \\ 0 & 0 & \frac{1}{\chi} + j(\frac{4}{3}\eta + \zeta)\omega \end{bmatrix} \begin{Bmatrix} u_1 \\ u_2 \\ u_3 \end{Bmatrix}.
 \end{aligned}$$

Consequently, six independent matrices are defined allowing for a more compact matrix formulation of the problem:

$$[A_{11}] = \begin{bmatrix} \frac{1}{j\chi\omega} + \frac{4}{3}\eta & 0 & 0 \\ 0 & \eta & 0 \\ 0 & 0 & \eta \end{bmatrix}, \quad [A_{12}] = \begin{bmatrix} 0 & \frac{1}{j\chi\omega} - \frac{2}{3}\eta & 0 \\ \eta & 0 & 0 \\ 0 & 0 & 0 \end{bmatrix},$$

$$[A_{13}] = \begin{bmatrix} 0 & 0 & \frac{1}{j\chi\omega} - \frac{2}{3}\eta \\ 0 & 0 & 0 \\ \eta & 0 & 0 \end{bmatrix},$$

$$[A_{22}] = \begin{bmatrix} \eta & 0 & 0 \\ 0 & \frac{1}{j\chi\omega} + \frac{4}{3}\eta & 0 \\ 0 & 0 & \eta \end{bmatrix}, \quad [A_{23}] = \begin{bmatrix} 0 & 0 & 0 \\ 0 & 0 & \frac{1}{j\omega\chi} - \frac{2}{3}\eta \\ 0 & \eta & 0 \end{bmatrix}, \quad (A2)$$

$$[A_{33}] = \begin{bmatrix} \eta & 0 & 0 \\ 0 & \eta & 0 \\ 0 & 0 & \frac{1}{j\chi\omega} + \frac{4}{3}\eta \end{bmatrix},$$

$$[A_{21}] = {}^t[A_{12}], \quad [A_{31}] = {}^t[A_{13}], \quad [A_{32}] = {}^t[A_{23}].$$

<sup>1</sup>D. Royer and E. Dieulesaint, *Elastic Waves in Solids* (Springer-Verlag, Berlin, 2000).

<sup>2</sup>J. Kestin and R. Dipippo, *American Institute of Physics Handbook*, 3rd ed. (McGraw-Hill, New York, 1982).

<sup>3</sup>R. N. Thurston, in *Wave Propagation in Fluids and Solids*, Physical Acoustics Vol. 1A, edited by W. P. Mason (Academic, New York, 1964).

<sup>4</sup>W. P. Mason, in *Piezoelectric Crystals and Mechanical Resonators*, Physical Acoustics Vol. 1A, edited by W. P. Mason (Academic, New York, 1964).

<sup>5</sup>T. A. Litovitz and C. M. Davis, in *Structural and Shear Relaxation in Liquids*, Physical Acoustics, Vol. 2A, edited by W. P. Mason (Academic, New York, 1965).

<sup>6</sup>A. H. Fahmy and E. Adler, *Appl. Phys. Lett.* **22**, 495 (1973).

<sup>7</sup>Th. Pastureaud, V. Laude, and S. Ballandras, *Appl. Phys. Lett.* **80**, 2544 (2002).

<sup>8</sup>A. Reinhardt, Th. Pastureaud, V. Laude, and S. Ballandras, *J. Appl. Phys.* **94**, 6923 (2003).

<sup>9</sup>S. Ballandras *et al.*, *J. Appl. Phys.* **96**, 7731 (2004).

<sup>10</sup>S. Camou, V. Laude, Th. Pastureaud, and S. Ballandras, *IEEE Trans. Ultrason. Ferroelectr. Freq. Control* **50**, 1363 (2003).

<sup>11</sup>G. Endoh, K. Hashimoto, and M. Yamaguchi, *Jpn. J. Appl. Phys., Part 1* **34**, 2638 (1995).

<sup>12</sup>K. Blötekjaer, K. A. Ingebrigsten, and H. Skeie, *IEEE Trans. Electron Devices* **ED-20**, 1133 (1973).